The Astrophysical Journal, 807:128 (13pp), 2015 July 10 doi:10.1088/0004-637X/807/2/128
© 2015. The American Astronomical Society. All rights reserved.

THE SCUBA-2 COSMOLOGY LEGACY SURVEY: ALMA RESOLVES THE BRIGHT-END OF THE SUB-MILLIMETER NUMBER COUNTS

J. M. Simpson[1], Ian Smail[1,2], A. M. Swinbank[1,2], S. C. Chapman[3], J. E. Geach[4], R. J. Ivison[5,6], A. P. Thomson[1], I. Aretxaga[7], A. W. Blain[8], W. I. Cowley[2], Chian-Chou Chen[1], K. E. K. Coppin[4], J. S. Dunlop[5], A. C. Edge[1], D. Farrah[9], E. Ibar[10], A. Karim[11], K. K. Knudsen[12], R. Meijerink[13], M. J. Michałowski[5], D. Scott[14], M. Spaans[15], and P. P. van der Werf[13]
[1] Centre for Extragalactic Astronomy, Department of Physics, Durham University, South Road, Durham DH1 3LE, UK; j.m.simpson@dur.ac.uk
[2] Institute for Computational Cosmology, Durham University, South Road, Durham DH1 3LE, UK
[3] Department of Physics and Atmospheric Science, Dalhousie University, Halifax, NS B3H 3J5, Canada
[4] Centre for Astrophysics Research, Science and Technology Research Institute, University of Hertfordshire, Hatfield AL10 9AB, UK
[5] Institute for Astronomy, University of Edinburgh, Royal Observatory, Blackford HIll, Edinburgh EH9 3HJ, UK
[6] European Southern Observatory, Karl Schwarzschild Strasse 2, Garching, Germany
[7] Instituto Nacional de Astrofísica, Óptica y Electrónica (INAOE), Luis Enrique Erro 1, Sta. María Tonantzintla, Mexico
[8] Department of Physics & Astronomy, University of Leicester, University Road, Leicester LE1 7RH, UK
[9] Department of Physics, Virginia Tech, Blacksburg, VA 24061, USA
[10] Instituto de Física y Astronomía, Universidad de Valparaíso, Avda. Gran Bretaña 1111, Valparaíso, Chile
[11] Argelander-Institute for Astronomy, Bonn University, Auf dem Hügel 71, D-53121 Bonn, Germany
[12] Department of Earth and Space Sciences, Chalmers University of Technology, Onsala Space Observatory, SE-43992 Onsala, Sweden
[13] Leiden Observatory, Leiden University, P.O. Box 9513, NL-2300 RA Leiden, The Netherlands
[14] Department of Physics & Astronomy, University of British Columbia, 6224 Agricultural Road, Vancouver, BC, V6T 1Z1, Canada
[15] Kapteyn Astronomical Institute, University of Groningen, The Netherlands
Received 2015 March 5; accepted 2015 May 18; published 2015 July 7

ABSTRACT

We present high-resolution 870 μm Atacama Large Millimeter/sub-millimeter Array (ALMA) continuum maps of 30 bright sub-millimeter sources in the UKIDSS UDS field. These sources are selected from deep, 1 degree^2 850 μm maps from the SCUBA-2 Cosmology Legacy Survey, and are representative of the brightest sources in the field (median $S_{\rm SCUBA\text{-}2} = 8.7 \pm 0.4$ mJy). We detect 52 sub-millimeter galaxies (SMGs) at >4σ significance in our 30 ALMA maps. In 61^{+19}_{-15}% of the ALMA maps the single-dish source comprises a blend of $\geqslant$2 SMGs, where the secondary SMGs are Ultra-luminous Infrared Galaxies (ULIRGs) with $L_{\rm IR} \gtrsim 10^{12}\,L_{\odot}$. The brightest SMG contributes on average 80^{+6}_{-2}% of the single-dish flux density, and in the ALMA maps containing $\geqslant$2 SMGs the secondary SMG contributes 25^{+1}_{-5}% of the integrated ALMA flux. We construct source counts and show that multiplicity boosts the apparent single-dish cumulative counts by 20% at $S_{870} > 7.5$ mJy, and by 60% at $S_{870} > 12$ mJy. We combine our sample with previous ALMA studies of fainter SMGs and show that the counts are well-described by a double power law with a break at 8.5 ± 0.6 mJy. The break corresponds to a luminosity of $\sim 6 \times 10^{12}\,L_{\odot}$ or a star formation rate (SFR) of $\sim 10^3\,M_{\odot}$ yr^{-1}. For the typical sizes of these SMGs, which are resolved in our ALMA data with $R_{\rm e} = 1.2 \pm 0.1$ kpc, this yields a limiting SFR density of $\sim 100\,M_{\odot}$ yr^{-1} kpc^{-2} Finally, the number density of $S_{870} \gtrsim 2$ mJy SMGs is 80 ± 30 times higher than that derived from blank-field counts. An over-abundance of faint SMGs is inconsistent with line-of-sight projections dominating multiplicity in the brightest SMGs, and indicates that a significant proportion of these high-redshift ULIRGs are likely to be physically associated.

Key words: galaxies: abundances – galaxies: high-redshift – galaxies: starburst – galaxies: star formation – submillimeter: galaxies

1. INTRODUCTION

The population of dusty galaxies that is detected at sub-millimeter (sub-mm) wavelengths, sub-millimeter galaxies (SMGs), represent some of the most intense sites of star formation in the universe. Sub-mm sources were first uncovered in surveys with SCUBA at the James Clerk Maxwell Telescope (JCMT; e.g., Smail et al. 1997; Barger et al. 1998; Hughes et al. 1998; Eales et al. 1999; Pope et al. 2005; Coppin et al. 2006), but subsequently studied at various facilities (e.g., Greve et al. 2004, 2008; Laurent et al. 2005; Scott et al. 2006; Bertoldi et al. 2007; Weiß et al. 2009; Austermann et al. 2010; Aretxaga et al. 2011; Lindner et al. 2011), and the radio-identified subset of the population has been shown to lie at a median redshift of $z \sim 2.3$ (Chapman et al. 2005). At these redshifts the typical flux densities of the sources ($S_{\nu} \sim 5$–15 mJy) correspond to total infrared luminosities of $\sim 10^{12}$–$10^{13}\,L_{\odot}$ (star formation rates (SFRs) of $\sim 10^2$–$10^3\,M_{\odot}$ yr^{-1}; see Magnelli et al. 2012; Swinbank et al. 2014), comparable to local Ultra-luminous Infrared Galaxies (ULIRGs). The importance of such prodigious SFRs, and thus rapid growth in stellar mass at high-redshift has led a number of authors to suggest that sub-mm sources represent a high-redshift phase in the evolution of local Elliptical galaxies (e.g., Lilly et al. 1999; Genzel et al. 2003; Blain et al. 2004; Swinbank et al. 2006; Tacconi et al. 2008; Hainline et al. 2011; Hickox et al. 2012; Simpson et al. 2014; Toft et al. 2014), highlighting their importance for models of galaxy formation.

Despite surveys with sub-mm/mm cameras such as SCUBA-2, LABOCA, AzTEC, or SPIRE on board *Herschel*, uncovering large numbers of sources, follow-up studies have been hampered by the coarse resolution delivered by these

single-dish facilities (typically 15″–30″ FWHM). At this resolution identifying the optical/near-infrared counterparts to the sub-mm emission (i.e., resolving the sub-mm source into its constituent SMGs) is challenging, a problem that is compounded by the expectation that these heavily dust-obscured galaxies are faint at optical wavelengths. One route to identifying the SMGs contributing to each sub-mm source has been to exploit the correlation between radio flux density and far-infrared emission in local galaxies, since 1.4 GHz imaging with the Very Large Array provides the sub-arcsecond resolution required to pin-point individual SMGs (e.g., Ivison et al. 1998, 2002, 2004, 2007; Smail et al. 2000; Bertoldi et al. 2007; Biggs et al. 2011; Lindner et al. 2011). Studies employing this method have successfully constrained the properties of ∼50% of the SMG population (Hodge et al. 2013b), but they do have limitations: this approach involves significant assumptions about the multi-wavelength properties of SMGs, and it is typically biased toward sources at lower redshift ($z \lesssim 2.5$) due to the positive K-correction at radio frequencies.

A further complication to the multi-wavelength identification procedure is caused by the potential blending of multiple individual SMGs into a single sub-mm source. Such source blending, or multiplicity, is somewhat expected given the coarse resolution of single-dish surveys, but is exacerbated by two further effects. First, the negative K-correction means that a sub-mm selection probes a large redshift range ($z \sim 1$–8), providing a significant path length for projection. Second, a number of studies have suggested that the intense star formation in SMGs is predominantly triggered by merger activity (e.g., Tacconi et al. 2008; Engel et al. 2010; Swinbank et al. 2010; Alaghband-Zadeh et al. 2012; Menéndez-Delmestre et al. 2013; Chen et al. 2015) and that the SMG population is strongly clustered (Blain et al. 2004; Scott et al. 2006; Weiß et al. 2009; Hickox et al. 2012, but see also Adelberger 2005; Williams et al. 2011). If SMGs are interacting, or reside in over-densities, then we may also expect to resolve sub-mm sources into physically associated (potentially interacting) pairs of SMGs. Indeed, studies of sub-mm sources that employ radio identifications often identify multiple *robust* counterparts to a single sub-mm source (e.g., Ivison et al. 2007), providing the first indication that multiplicity is a non-negligible effect.

Prior to the Atacama Large Millimeter/sub-millimeter Array (ALMA), sub-mm interferometry with facilities such as the Plateau de Bure Interferometer (PdbI) or Sub-millimeter Array (SMA) offered the only definitive route to identify the SMGs contributing to single-dish detected sub-mm sources. However, while these facilities provide the ∼1″–2″ resolution necessary to locate SMGs, their sensitivity meant that follow-up observations were typically only possible for a handful of the brightest sub-mm sources (e.g., Gear et al. 2000; Iono et al. 2006; Younger et al. 2007, 2009; Wang et al. 2007, 2011; Dannerbauer et al. 2008; Cowie et al. 2009; Aravena et al. 2010; Barger et al. 2012; Smolčić et al. 2012; Chen et al. 2013b; Ivison et al. 2013), and often at different wavelengths to the initial single-dish selection. The first conclusive evidence of multiplicity in sub-mm sources was presented by Wang et al. (2011), who used observations with the SMA to show that two bright sub-mm sources were comprised of blends of 2 or 3 individual SMGs, with flux densities of $S_{850} = 3$–5 mJy, and thought to be at different redshifts.

Building upon this result, Barger et al. (2012) used the SMA to observe 16 SCUBA-detected sources in the GOODS-N field, at ∼2″ resolution. The observations resolve three of the sub-mm sources into multiple SMGs, leading the authors to conclude that ∼40% of SMGs brighter than 7 mJy may be blends of multiple SMGs. However, the SMA observations have a typical depth of $\sigma_{860} \sim 0.6$–1 mJy, hence only being sensitive to secondary SMGs brighter than 3–4 mJy, and the small number of sources in the sample leads to significant uncertainties on the multiplicity fraction. In a similar study, Smolčić et al. (2012) showed that 6/28 LABOCA 870 μm sources are comprised of blends of SMG in 1.3 mm follow-up observations with the PdBI, with a further nine sources not detected.

The commissioning of ALMA promises a revolution in our understanding of the SMG population. Indeed, even with the limited capabilities available in Cycle-0, Hodge et al. (2013b) obtained robust observations of 88 single-dish sources detected at 870 μm in the LABOCA survey of the Extended *Chandra* Deep Field South (LESS). These ALMA, 1.″5 resolution, "snapshot" observations pin-pointed the SMGs contributing to the LABOCA sources and showed that at least 35% of the sources are comprised of ⩾2 SMGs. Furthermore, to recover the LABOCA flux density, Hodge et al. (2013b) also showed it is necessary to include flux in faint sources below their nominal detection threshold, indicating that a significant proportion of the ALMA maps contain additional faint 1–2 mJy SMGs.

One key result from this ALMA-LESS (ALESS) survey is that despite the sample containing 12 LABOCA sources above 9 mJy, only one ALMA-detected SMG is brighter than this limit. As a result, Karim et al. (2013) conclude that due to multiplicity the bright-end of the sub-mm number counts may have been significantly over-estimated in single-dish surveys, suggesting a cut off in the SFR in the most luminous starbursts corresponding to a potential Eddington limit at 9 mJy (equivalent to a SFR of $\sim 10^3\,M_\odot\,\mathrm{yr}^{-1}$). Although a number of SMGs above this threshold have been detected in previous interferometric surveys (e.g., Younger et al. 2007, 2009; Barger et al. 2012; Chen et al. 2013b).

To improve the statistics of multiplicity in the brightest sub-mm sources we have obtained ALMA 870 μm follow-up observations of 30 bright (850 μm selected) sub-mm sources in the UKIDSS Ultra Deep Survey (UDS) field (Lawrence et al. 2007). These single-dish targets were selected from deep, wide-field observations taken as part of the SCUBA-2 Cosmology Legacy Survey (S2CLS) at the JCMT (14.″5 FWHM resolution), and are representative of the brightest sources in the field (J.E. Geach et al. 2015, in preparation). We use the data to measure the multiplicity in the single-dish population, probe the bright-end of the number counts and investigate the number density of secondary SMGs.

The paper is structured as follows. In Section 2 we discuss our sample selection, the ALMA observations, and our data reduction. In Section 3 we describe the construction of our source catalog and provide a comparison between the ALMA and SCUBA-2 detections. In Section 4 we discuss the fraction of the single-dish sources that fragment into multiple SMGs and present the *resolved* number counts. Our conclusions are given in Section 5. We adopt a cosmology with $H_0 = 71\ \mathrm{km\ s^{-1}\ Mpc^{-1}}$, $\Omega_\Lambda = 0.73$, and $\Omega_\mathrm{m} = 0.27$. Throughout this work error estimates are from a bootstrap analysis, unless otherwise stated.

2. OBSERVATIONS AND DATA REDUCTION

2.1. Sample Selection

The sub-mm sources in this paper were selected from observations taken as part of the S2CLS programme at the JCMT. The latest S2CLS map of the UDS field (as of 2014 August) reaches a uniform depth of $\sigma_{850} = 1.3$ mJy across 0.78 deg^2. However, our initial sample selection for the Cycle-1 deadline in early 2013 was made from the first version of these observations (2013 February), which reached a 1–σ_{850} depth of 2.0 mJy. From these earlier observations we selected 31 sources detected at >4σ, and hence having observed 850 μm flux densities of >8 mJy. We removed one source from our sample that is a bright, lensed, SMG with previous interferometric follow-up observations (Ikarashi et al. 2011), leaving a sample of 30 targets (see Figure 1). We note that the sources are extracted from a beam-smoothed SCUBA-2 map (i.e., matched-filtered), which has a resulting spatial resolution of 20.″5 (i.e., $\sqrt{2} \times 14.''5$)

In Figure 2 we show the flux density distribution for the 30 sources in our sample, measured from the deeper 2014 August S2CLS map of the UDS field ($\sigma_{850} = 1.3$ mJy). In the deeper imaging 12/30 of the sub-millimeter sources scatter to lower flux densities ($S_{850} < 8$ mJy), with 2 sources not detected above our 3.5σ detection threshold (although both ALMA maps contain SMGs). While we present the ALMA observations of these 2 "sources" (UDS 298 and 392), we note that formally 28 of the sources in our sample are now single-dish-detected. Overall our sample consists of 850 μm-bright sub-mm sources, with a median observed (i.e., not deboosted) flux density of (8.7 ± 0.4) mJy. The completeness of our sample relative to the new, deeper catalog is >50% at $S_{850} > 8$ mJy, and 100% at $S_{850} > 11$ mJy over this 0.8 deg^2 field.

2.2. Data Reduction

We obtained ALMA 870 μm (Band 7) continuum imaging of all 30 targets from our sample on 2013 November 1, as part of the Cycle-1 project 2012.1.00090.S. All targets were observed using 7.5 GHz of bandwidth centered at 344 GHz (870 μm), chosen to match the frequency of the original SCUBA-2 observations. We used a "single continuum" correlator setup with four basebands of 128 dual-polarization channels each. The FWHM primary beam of ALMA is 17.″3 at our observing frequency, and we centered the observations at the position of the sub-mm sources in the 2013 February SCUBA-2 map. The ALMA primary beam (FWHM) is comparable to the spatial resolution of the beam-smoothed SCUBA-2 map (FWHM = 20.″5) and hence our observations are able to detect the majority of SMGs that contribute significantly to the single-dish source.

The observations were conducted using 26 12 m antennae with a range of baselines from 20 to 1250 m, and a median baseline of 200 m. The array configuration yields a synthesized beam of $0.''35 \times 0.''25$ using Briggs weighting (robust parameter = 0.5), at a P.A. of ~55° for our observations. The observing strategy involved our 30 targets being observed in two measurement sets, each containing 15 unique targets. Each measurement set contains seven or eight sub-blocks, consisting of 30 s observations of ten targets. In total each target was observed five times (total integration time of 150 s), with each repeat distributed randomly within these sub-blocks. Calibration observations were taken between each sub-block, with 90 s phase calibration observations (J0217+014; $S_{870} = 0.49$ Jy) and 30 s atmospheric calibrations. The absolute flux scale for each measurement set was derived from observations of J0238+166, and either J0423–0120 or J0006–0623 was used for bandpass calibration. The flux density of the amplitude calibrator was set at 0.59 Jy, but we note that the ALMA calibrator archive shows that this source has day-to-day variations of up to 10%.

The calibration and imaging of our science targets, and calibrators, was performed using the Common Astronomy Software Application (casa version 4.2.1).[16] To image each target we first Fourier transform the *uv*-data to create a "dirty" map, using Briggs weighting (robust parameter = 0.5). Following Hodge et al. (2013b) we determine the amount of cleaning required based on the presence of strong sources in the maps. We first estimate the rms in each dirty map and clean the map to 3σ. We then measure the rms in the cleaned map and identify any sources above 5σ. If a source is detected at >5σ then we repeat the cleaning process but place a tight clean box around each >5σ source and clean the dirty map to 1.5σ. If a map does not contain any >5 σ sources then the map cleaned to 3σ is considered the final map. The final maps have a range of 1–σ_{870} depths from 0.19 to 0.24 mJy beam^{-1} (median $\sigma_{870} =$ 0.21 mJy beam^{-1}).

Long wavelength studies to resolve SMGs, either in the sub-mm, radio, or molecular line emission (i.e., ^{12}CO), suggest that we may risk resolving the SMGs in our high-resolution ALMA maps (see Chapman et al. 2004; Tacconi et al. 2006; Biggs & Ivison 2008; Bothwell et al. 2010; Engel et al. 2010; Younger et al. 2010; Simpson et al. 2015). Hence, to ensure that any extended flux from the SMGs is not resolved-out, and that we detect low surface brightness, extended, sources, we repeated the imaging process using natural weighting, and applied a 0.″6 Gaussian taper in the *uv*-plane; using a Gaussian taper down-weights visibilities on long baselines, yielding a larger synthesized beam, which increases the sensitivity to extended sources, at the cost of increased noise in the map. The maps were then imaged, and cleaned, using the same procedure described above to create a set of low-resolution "detection" maps. These low-resolution "detection" maps have a median rms of $\sigma_{870} = 0.26$ mJy beam^{-1} and a median synthesized beam of $0.''8 \times 0.''65$. Both the "detection" and higher resolution maps have a size of $36'' \times 36''$, and a pixel scale of 0.″04.

3. SOURCE EXTRACTION

To construct a source catalog from our ALMA maps we use the source extraction package sextractor (v2.8.6; Bertin & Arnouts 1996). We search the low-resolution 0.″8 "detection" maps and identify all >3σ "peaks" in the non-primary-beam corrected maps. At the position of each >3σ detection we measure both the peak flux density and the integrated flux density in a 0.″8 radius aperture. We also measure integrated flux densities in the higher resolution maps, at the position of all the detected sources in the 0.″8 resolution maps. The fluxes measured in both sets of maps are primary-beam corrected using the model of the primary beam response output by casa. The integrated flux densities of the calibrators, in the 0.″8 radius aperture, are 4% lower than the total flux density

[16] We repeated the data reduction using the most recent version of casa (4.2.2) and found it had no effect on our final maps or source catalog.

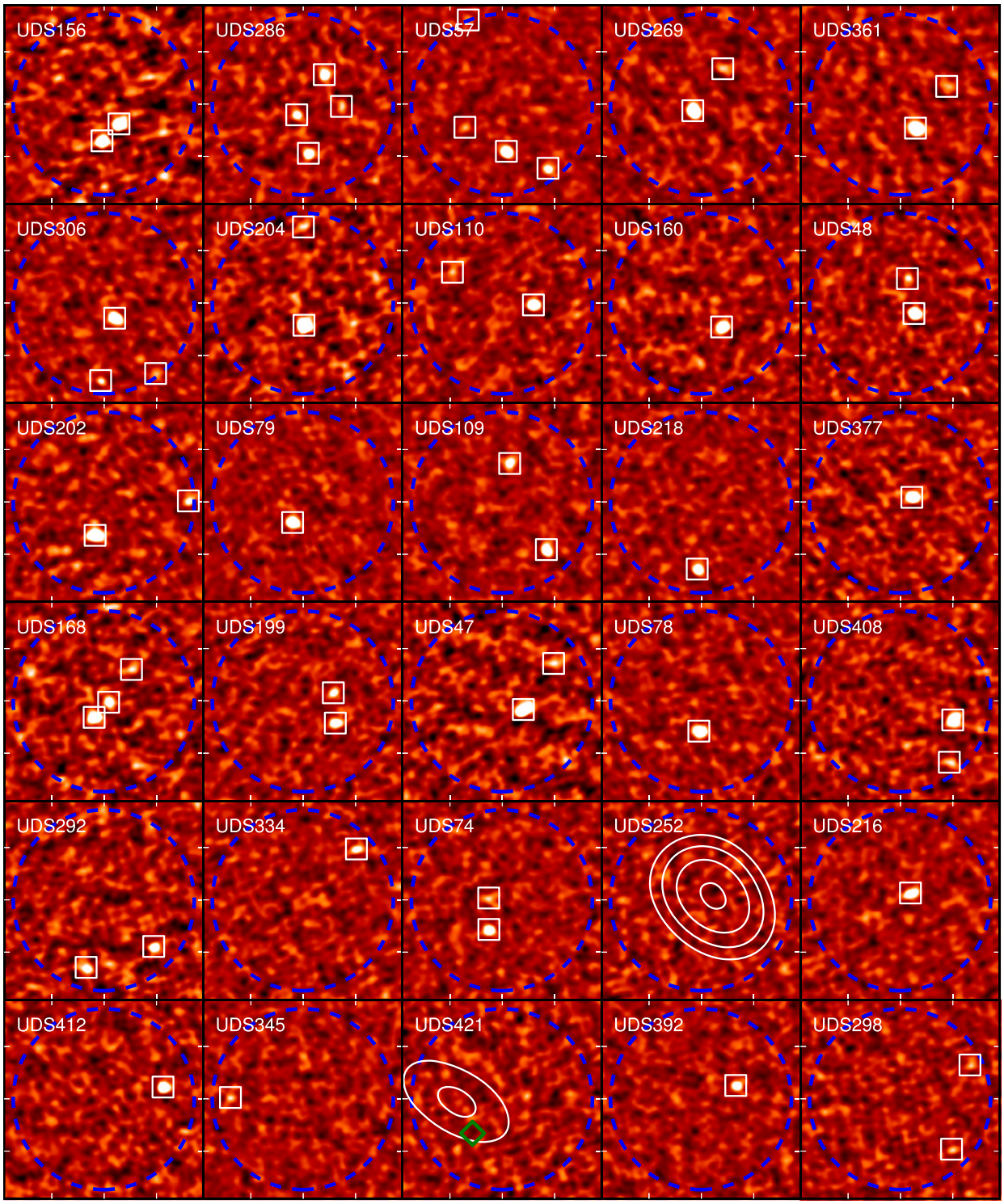

Figure 1. ALMA 870 μm continuum maps, at 0.″8 resolution, of 30 bright sub-mm sources in the UDS field. These sources are selected to be representative of the brightest sources detected in the S2CLS survey of this ~0.8 deg^2 field. The 18″ × 18″ non-primary-beam-corrected maps (roughly 150 kpc × 150 kpc at the typical SMG redshift, $z = 2.5$) are ordered by decreasing single-dish flux density and have a median 1-σ rms of 0.26 mJy beam^{-1}. The dashed circle on each thumbnail represents the primary beam (FWHM) of ALMA at 870 μm. We detect 52 SMGs at >4σ (marked by a squares) in the 30 ALMA maps, with 870 μm flux densities of 1.3–12.9 mJy. In 18/30 ALMA maps the single-dish sub-mm source fragments into two or more individual SMGs. In particular, we highlight UDS 57, 168, 286 and 306, where the ALMA observations demonstrate that the single-dish source is comprised of three-or-four SMGs. In two ALMA maps, UDS 252 and 421, we do not detect any SMGs, but note that both SCUBA-2 sources are detected in *Herschel*/SPIRE imaging. We plot contours representing the single-dish SCUBA-2 emission at 3, 3.5, 4.0, 4.5 × σ for these sources, note that UDS 421 has a potential VLA/1.4 GHz counterpart (diamond; Arumugan et al. submitted) that is not detected in our ALMA maps.

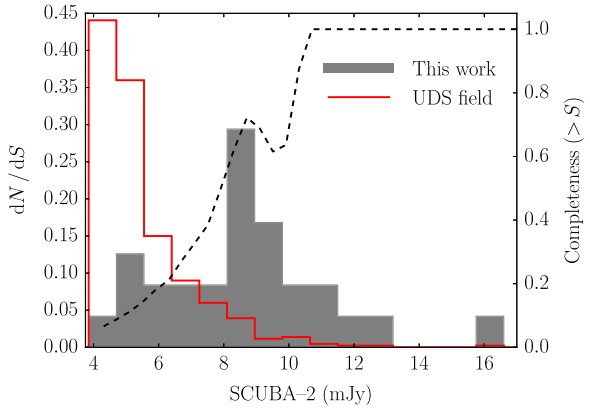

Figure 2. 850 μm flux distribution of the single-dish-identified sub-mm sources targeted with ALMA (shaded histogram) compared to the flux distribution of sub-mm sources in the UDS field (open histogram). Both distributions are normalized by the total number of sources in each sample. A dashed line shows the completeness of our sample, relative to the latest single-dish catalog (right-hand axis). While our observations do not represent a flux-limited sample in the new S2CLS map, we note that they are clearly weighted to the bright-end of the sub-mm population. The ALMA sample is >50% complete for single-dish sources brighter than 8 mJy, and 100% complete at >11 mJy.

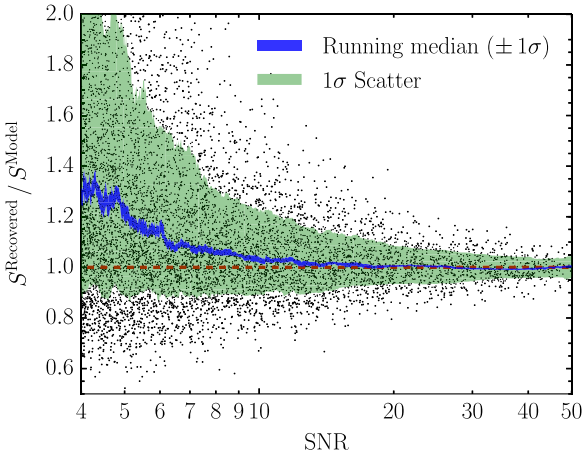

Figure 3. Results of simulations involving injecting fake sources into our source-subtracted ALMA maps to test the reliability of our source extraction procedure. Here we show the ratio of the recovered to input source flux density as a function of output source SNR, where the flux density of each model source is drawn from a steeply declining power-law distribution (with an index of −2). We show the running median and associated 1-σ bootstrap uncertainty, along-with the 1σ scatter. At our detection threshold of 4σ the flux of individual sources is on average boosted by 30%, falling to <10% at >6σ and <1% at >15σ.

measured using the CASA IMFIT routine, and we apply this correction to the integrated flux densities of the SMGs.

Although we extract sources above 3σ, we expect a catalog at this SNR limit to contain some spurious detections. To estimate the level of contamination we invert the 0.″8 resolution "detection" maps and repeat the source extraction. Within the FWHM primary beam the number of negative detections is lower than positive sources at >3.5σ, but the contamination is 50% at 3.5–4.0σ (falling to 10% at 4.0–4.5σ). The number of sources detected across all 30 inverted maps is $\leqslant$1 at >4σ (corresponding to a contamination of 2% when considering our entire catalog) and we therefore adopt this as the detection threshold for our source catalog. Applying a 4σ cut to our source catalog yields 52 SMGs (see Table 1), within the FWHM primary beam of the 30 ALMA maps. A search for sources outside the ALMA primary beam does not identify any statistically significant detections. We detect no SMGs in 2 ALMA maps (UDS 252 and 421) and a single SMG in a further 10 maps. However, in most of the ALMA maps we detect multiple SMGs and 14, 2, and 2 of the maps contain 2, 3, or 4 SMGs, respectively.

We perform a number of tests to investigate whether the sources are resolved in the ALMA imaging. These are detailed in Simpson et al. (2015), but we give a summary here. First, we measure the ratio of the peak flux in the 0.″3 and 0.″8 resolution maps. The peak flux of the SMGs is lower in the 0.″3 resolution maps, with a median ratio of $S^{0.3}_{\rm pk}/S^{0.8}_{\rm pk} = 0.65 \pm 0.02$, indicating that the sources are resolved in the higher resolution imaging. second, we investigate the ratio of the integrated-to-peak flux density in the 0.″8 maps; if the sources are unresolved the peak flux density will equal the integrated flux density. The median ratio of peak-to-total flux in the 0.″8 imaging is 0.82 ± 0.03, again indicating that the sources are marginally resolved at 0.″8 resolution. Finally, we fit point-source and extended models to the sub-mm emission at both resolutions and find that a point-source model results in significant residuals, and is insufficient to describe the emission from these sources. We also show that the sizes derived from the model fitting are consistent with the properties of the SMGs in the *uv*-plane (Simpson et al. 2015). We therefore take the flux density of each SMG to be the integrated flux measured in the 0.″8 maps, unless it is lower than the peak flux density.

3.1. Completeness and Reliability

To test the completeness and reliability of our source extraction we create 2×10^4 simulated ALMA maps. However, to ensure that we have realistic noise properties we start with one pair (i.e., at 0.″3 and 0.″8 resolution) of our source-subtracted ALMA maps. To these we then add a model source at the same, but random, position in both resolution maps. The flux densities of the model sources are drawn randomly from a steeply declining power-law distribution (with an index of −2; consistent with Karim et al. 2013), and have peak SNR values of 2–50σ. The intrinsic FWHM size of each model source is drawn from a uniform distribution from 0–0.″5, and we convolve each model source with the ALMA synthesized beam. To simulate realistic noise, we add the convolved source to a random position in one pair (i.e., at 0.″3 and 0.″8 resolution) of our source-subtracted ALMA maps.

We perform the source extraction procedure described above on each simulated map and consider a source recovered if it is detected within 0.″8 of the injected position. The completeness is 93% at >4σ, rising to about 100% at 5.5σ, consistent with the results of similar studies (e.g., Karim et al. 2013; Ono et al. 2014).

In Figure 3 we show the ratio of output-to-input flux density for our simulated sources. The flux densities of sources in a signal-to-noise limited catalog are known to be boosted if the sources are drawn from a non-uniform flux distribution. The effect, known as flux boosting, arises due to more sources scattering upwards in flux density, because of random noise fluctuations, than scatter down as a result of the steeply rising source counts (see also Hogg & Turner 1998; Scott et al. 2002; Coppin et al. 2006; Weiß et al. 2009). On average a 4σ detection in our ALMA maps is boosted in flux by 30%, with

the boost falling to <10% at >6σ and <1% at >15σ. This flux boosting is sensitive to the slope of the power law that defines the flux distribution of the sources, and we note that varying the slope within the 1-σ uncertainties presented by Karim et al. (2013) changes the correction by $\pm$10% at a detection limit of 4σ. We also measure the peak and integrated flux densities of the simulated sources at both resolutions and find that the flux boosting correction does not affect our conclusion that the SMGs in our sample are resolved in the high-resolution imaging.

To correct the measured flux densities of the 52 SMGs detected in our ALMA imaging for flux boosting we calculate the median ratio of output-to-input flux for the simulated sources in bins of 0.25σ. We fit a spline to the median of each bin, and correct the flux densities in our catalog based on the SNR of each source and the spline fit (Figure 3). Our final source catalog thus consists of 52 SMGs, with a range of deboosted 870 μm flux densities of 1.3–12.9 mJy beam^{-1}, detected in 30 ALMA maps targeting the brighter single-dish sub-mm sources from the 0.8 deg^2 S2CLS UDS field.

3.2. Astrometry and Flux Recovery

We first compare the flux integrated across all sources in our maps to that seen by SCUBA-2, to test if our catalog is missing large numbers of faint sources or if we are missing very extended sub-mm emission. We also use our catalog to test the astrometry of the SCUBA-2 map. For each ALMA map we create a model of the detected SMGs using their primary-beam-corrected flux densities and convolve each ALMA model map with a model of the SCUBA-2 beam. The model beam is consistent with a beam created by stacking of bright SMGs in the UDS field, and with calibrator observations. These convolved ALMA maps do not take into account the contribution to the SCUBA-2 detection from sources either below the ALMA detection threshold, or outside the primary beam. It also neglects any effect due to the different bandwidth of the SCUBA-2 (35 GHz half-power bandwidth) and ALMA (2 × 4 GHz) observations. However, it provides a reasonable test of the effect of a 20 × improvement in resolution that our ALMA observations provide, relative to SCUBA-2.

We measure a small, systematic, offset in both R.A. and decl. of $-0.6^{+0.3}_{-0.3}$″ and $-1.1^{+0.2}_{-0.5}$″, respectively (in the sense ALMA-SCUBA-2), amounting to less than the fiducial pixel size of the SCUBA-2 map (2″). As expected, the separation between the SCUBA-2 source and the convolved ALMA map centroid is a function of the SNR of the single-dish detection (Figure 4). Importantly, the measured separations are consistent with the expected single-dish positional uncertainties: 70% of the separations are smaller than the predicted 1σ uncertainty on the single-dish position given by Equation (B22) from Ivison et al. (2007). These offsets are between the SCUBA-2 and convolved ALMA peak positions, and hence only represent the expected search radius for a single, isolated, counterpart to the single-dish emission (i.e., an ALMA map with a single detected SMG). However, the median separation between the brightest SMG in each map and the SCUBA-2 detection is $1.7^{+0.6}_{-0.2}$″, which is consistent with (although with a marginally increased scatter) the median separation of the convolved ALMA map centroids and the SCUBA-2 positions ($1.6^{+0.2}_{-0.2}$″). These results indicate that the offset to the brightest SMG is consistent with the SNR-based search radius used to identify counterparts to a sub-mm source, prior to interferometric observations in the sub-mm (e.g., Ivison et al. 2007).

To confirm the relative flux scales, and also to test that the observations have not resolved-out flux or missed large numbers of faint SMGs, we compare the peak flux density of the convolved ALMA maps to the SCUBA-2 detections (see Figure 4). The median ratio of the ALMA-to-SCUBA-2 flux is $S^{\rm ALMA}/S^{\rm SCUBA\text{-}2} = 0.99^{+0.10}_{-0.04}$, including upper limits for a source at the edge of the primary beam in the ALMA "blank" maps. The result indicates good agreement between flux scales, and suggests that all of the SMGs that contribute significantly to the single-dish flux density are recovered within the 17.″3 ALMA primary-beam (compared to the 20.″5 resolution of the beam-convolved SCUBA-2 map from which the sources are extracted). We note that we have not applied a deboosting correction to the SCUBA-2 flux densities. The deboosting curve for 850 μm SCUBA-2 observations presented by Chen et al. (2013a) indicates that the median deboosting correction for our sample of bright sources is ∼10%. However, we stress that the systematic uncertainty on the absolute flux calibration of both SCUBA-2 and ALMA are expected to be comparable, or higher than, the deboosting correction. Indeed, the systematic uncertainty on the SCUBA-2 flux density scale is estimated to be 5%–10% (Dempsey et al. 2013), while the absolute flux density of the ALMA observations is sensitive to the properties of the amplitude calibrator chosen. We note that the ALMA data presented here is calibrated to a Quasar, J0238+166, which, as shown in the ALMA calibration archive, has daily variations of up to 10% in addition to the systematic calibration uncertainties. Given these large systematic uncertainties we simply note that the flux density scales of the SCUBA-2 and ALMA data appear well-matched with our current analysis.

4. DISCUSSION

4.1. Multiplicity

Previous interferometric follow-up studies of sub-mm sources have hinted that a fraction of the sources may be comprised of multiple individual SMGs, which appear blended in the $\gtrsim$15″ resolution single-dish imaging (e.g., Tacconi et al. 2006; Ivison et al. 2007; Wang et al. 2011; Barger et al. 2012; Smolčić et al. 2012; Hodge et al. 2013b). Such an effect is expected, given the low resolution of single-dish sub-mm maps, but prior to ALMA the effect has been challenging to quantify due to the small sample sizes, mixed wavelength of observations, and the limited sensitivity of follow-up studies.

It is evident from the ALMA maps presented in Figure 1 that a significant proportion of the single-dish sub-mm sources in our sample are comprised of multiple, $S_{870} > 1$ mJy, SMGs. Indeed, 17 of the 28 SCUBA-2 detected sources fragment into >1 SMGs, a multiple fraction of 61^{+19}_{-15}% if we consider any secondary component, and assuming poisson uncertainties. In particular we highlight UDS 57, 168, 286, and 306 where the single-dish sub-mm sources are a blend of 3 or 4 SMGs. Hence, each of these maps contains multiple ULIRGs ($S_{870} \gtrsim 1$ mJy) with a SFR [17] of $\gtrsim$150 $M_\odot$ yr^{-1}.

Defining multiplicity by the number of companions is clearly dependent on the sensitivity limit for these secondary

[17] Assuming a typical conversion between 870 μm flux density and FIR-luminosity (e.g., Swinbank et al. 2014), and a Salpeter Initial Mass Function (IMF).

Table 1
Source Properties

ID	R.A. (J2000)	Decl. (J2000)	$\sigma_{\rm ALMA}$ (mJy beam^{-1})	$S_{\rm obs}^{\rm SCUBA\text{-}2}$ (mJy)	S/N$_{\rm peak}^{\rm ALMA}$	$S_{\rm obs}^{\rm ALMA}$ (mJy)	Deboosting[b] Correction	FWHM[c] ($''$)
UDS156.0	2:18:24.14	−5:22:55.3	0.34	16.1 ± 1.2	24.5	9.7 ± 0.7	1.00	0.25 ± 0.02
UDS156.1	2:18:24.24	−5:22:56.9	0.34	16.1 ± 1.2	20.0	8.5 ± 0.7	1.00	0.24 ± 0.03
UDS286.0	2:17:25.73	−5:25:41.2	0.30	12.4 ± 1.2	13.3	5.2 ± 0.7	0.98	...
UDS286.1	2:17:25.63	−5:25:33.7	0.30	12.4 ± 1.2	12.9	5.1 ± 0.6	0.98	0.26 ± 0.07
UDS286.2	2:17:25.80	−5:25:37.5	0.30	12.4 ± 1.2	8.6	2.7 ± 0.6	0.95	...
UDS286.3	2:17:25.52	−5:25:36.7	0.30	12.4 ± 1.2	4.6	1.7 ± 0.6	0.80	...
UDS57.0	2:19:21.14	−4:56:51.3	0.26	12.1 ± 1.2	26.3	9.5 ± 0.6	1.00	0.34 ± 0.02
UDS57.1	2:19:20.88	−4:56:52.9	0.26	12.1 ± 1.2	10.5	6.0 ± 0.9	0.97	0.26 ± 0.05
UDS57.2	2:19:21.41	−4:56:49.0	0.26	12.1 ± 1.2	4.9	1.8 ± 0.6	0.82	...
UDS57.3	2:19:21.39	−4:56:38.8	0.26	12.1 ± 1.2	4.2	2.7 ± 1.0	0.78	...
UDS269.0	2:17:30.44	−5:19:22.4	0.29	11.4 ± 1.2	33.8	12.9 ± 0.6	1.00	...
UDS269.1	2:17:30.25	−5:19:18.4	0.29	11.4 ± 1.2	4.5	2.6 ± 0.7	0.79	...
UDS361.0	2:16:47.92	−5:01:29.8	0.27	11.4 ± 1.2	25.8	11.8 ± 0.6	1.00	0.62 ± 0.02
UDS361.1	2:16:47.73	−5:01:25.8	0.27	11.4 ± 1.2	4.2	2.6 ± 0.7	0.77	...
UDS306.0	2:17:17.07	−5:33:26.6	0.24	10.5 ± 1.3	28.7	8.3 ± 0.5	1.00	0.30 ± 0.02
UDS306.1	2:17:17.16	−5:33:32.5	0.24	10.5 ± 1.3	6.6	2.6 ± 0.4	0.90	...
UDS306.2	2:17:16.81	−5:33:31.8	0.24	10.5 ± 1.3	4.0	3.0 ± 0.9	0.76	...
UDS204.0	2:18:03.01	−5:28:41.9	0.31	10.4 ± 1.2	27.6	11.6 ± 0.6	1.00	0.58 ± 0.02
UDS204.1	2:18:03.01	−5:28:32.5	0.31	10.4 ± 1.2	4.1	2.9 ± 0.9	0.77	...
UDS110.0	2:18:48.24	−5:18:05.2	0.30	9.5 ± 1.2	22.5	7.7 ± 0.6	1.00	0.28 ± 0.02
UDS110.1	2:18:48.76	−5:18:02.1	0.30	9.5 ± 1.2	4.3	2.5 ± 0.8	0.78	...
UDS160.0	2:18:23.73	−5:11:38.5	0.30	9.5 ± 1.2	20.8	7.9 ± 0.6	1.00	...
UDS48.0	2:19:24.57	−4:53:00.2	0.24	9.4 ± 1.1	28.4	7.5 ± 0.5	1.00	0.28 ± 0.02
UDS48.1	2:19:24.62	−4:52:56.9	0.24	9.4 ± 1.1	5.6	1.6 ± 0.5	0.86	...
UDS202.0	2:18:05.65	−5:10:49.6	0.25	9.3 ± 1.2	27.7	10.5 ± 0.5	1.00	0.36 ± 0.02
UDS202.1	2:18:05.05	−5:10:46.3	0.25	9.3 ± 1.2	6.5	3.9 ± 0.9	0.90	...
UDS79.0	2:19:09.94	−5:00:08.6	0.24	8.9 ± 1.2	23.8	7.7 ± 0.5	1.00	0.43 ± 0.02
UDS109.0	2:18:50.07	−5:27:25.5	0.26	8.8 ± 1.2	16.0	7.7 ± 0.7	0.99	...
UDS109.1	2:18:50.30	−5:27:17.2	0.26	8.8 ± 1.2	9.6	4.3 ± 0.6	0.97	...
UDS218.0	2:17:54.80	−5:23:23.0	0.23	8.7 ± 1.2	17.0	6.6 ± 0.7	1.00	0.37 ± 0.04
UDS377.0	2:16:41.11	−5:03:51.4	0.26	8.7 ± 1.2	28.5	8.1 ± 0.5	1.00	0.16 ± 0.02
UDS168.0	2:18:20.40	−5:31:43.2	0.30	8.7 ± 1.2	17.3	6.7 ± 0.6	1.00	0.42 ± 0.03
UDS168.1	2:18:20.31	−5:31:41.7	0.30	8.7 ± 1.2	7.0	3.0 ± 0.6	0.92	...
UDS168.2	2:18:20.17	−5:31:38.6	0.30	8.7 ± 1.2	4.2	2.0 ± 0.7	0.78	...
UDS199.0	2:18:07.18	−4:44:13.8	0.26	8.6 ± 1.2	13.4	4.3 ± 0.6	0.98	0.28 ± 0.06
UDS199.1	2:18:07.19	−4:44:10.9	0.26	8.6 ± 1.2	8.7	2.5 ± 0.5	0.96	...
UDS47.0	2:19:24.84	−5:09:20.7	0.31	8.4 ± 1.2	21.7	8.7 ± 0.6	1.00	0.28 ± 0.03
UDS47.1	2:19:24.64	−5:09:16.3	0.31	8.4 ± 1.2	4.0	2.7 ± 0.8	0.76	...
UDS78.0	2:19:09.74	−5:15:30.6	0.25	7.6 ± 1.2	22.9	8.2 ± 0.5	1.00	0.35 ± 0.03
UDS408.0	2:16:22.26	−5:11:07.8	0.28	7.6 ± 1.2	17.9	9.1 ± 0.7	1.00	0.66 ± 0.04
UDS408.1	2:16:22.28	−5:11:11.9	0.28	7.6 ± 1.2	4.5	2.7 ± 0.9	0.79	...
UDS292.0	2:17:21.53	−5:19:07.8	0.28	6.7 ± 1.2	9.7	4.2 ± 0.8	0.97	...
UDS292.1	2:17:21.96	−5:19:09.8	0.28	6.7 ± 1.2	6.9	3.9 ± 0.8	0.91	...
UDS334.0	2:17:02.47	−4:57:20.0	0.27	6.7 ± 1.2	7.5	3.8 ± 0.8	0.93	...
UDS74.0	2:19:13.19	−4:47:08.0	0.24	6.0 ± 1.2	15.2	4.6 ± 0.5	0.98	0.38 ± 0.04
UDS74.1	2:19:13.19	−4:47:05.0	0.24	6.0 ± 1.2	4.8	1.8 ± 0.5	0.81	...
UDS216.0	2:17:56.74	−4:52:38.9	0.28	5.2 ± 1.2	14.5	5.3 ± 0.5	0.98	0.70 ± 0.04
UDS412.0	2:16:20.13	−5:17:26.2	0.25	5.1 ± 1.2	17.2	6.6 ± 0.7	1.00	0.30 ± 0.07
UDS345.0	2:16:57.61	−5:20:38.6	0.24	4.8 ± 1.2	5.3	2.3 ± 0.7	0.84	...
UDS392.0[a]	2:16:33.29	−5:11:59.0	0.23	<4.1	13.3	3.8 ± 0.5	0.98	<0.18
UDS298.0[a]	2:17:19.57	−5:09:41.2	0.24	<4.1	4.4	1.6 ± 0.4	0.79	...
UDS298.1[a]	2:17:19.46	−5:09:33.2	0.24	<4.1	4.2	2.1 ± 0.8	0.78	...

Notes.
[a] Source is not detected by SCUBA-2.
[b] The intrinsic flux densities of the ALMA SMGs are obtained by multiplying $S_{\rm obs}^{\rm ALMA}$ with the deboosting correction.
[c] Intrinsic source size, corrected for synthesized beam (see Simpson et al. 2015). Sizes are only measured for SMGs detected at >10σ.

components. However, adopting a limit of $S_{870} > 1$ mJy measures the number of ULIRGs that contribute to each single-dish sub-mm source, is reasonably well-matched to the depth of our maps and is sufficiently bright that we would expect to detect <1 SMG by chance in our 30 survey fields based on the blank field counts (see Figure 6). As we show in Section 4.4 the number density of these secondary SMGs appears to be higher than that expected in random fields or from simple selection biases, indicating that a fraction of these multiples are likely to be physically associated.

Table 2
Cumulative 870 μm Number Counts

S_{870} (mJy)	$N(>S_{870})$ (deg^{-2})
7.5	$51.6^{+15.8}_{-12.4}$
9.0	$15.8^{+8.5}_{-5.8}$
10.5	$5.8^{+5.6}_{-3.1}$
12.0	$1.7^{+4.0}_{-1.4}$

It is interesting to note that 2 of our ALMA maps are blank, i.e., we do not detect any SMGs at >4σ. Although the sub-mm sources targeted in these maps (UDS 252 and 421) are two of the fainter SCUBA-2 sources in our sample (4.4 and 5.6 mJy) they are detected in both the 2013 February and 2014 August SCUBA-2 maps, as well as in 250, 350, and 500 μm *Herschel*/SPIRE imaging (50 and 26 mJy at 250 μm, respectively), indicating that they are not simply spurious SCUBA-2 detections. A simple explanation (given that 17 of our ALMA maps contain multiple SMGs) is that in these maps the single-dish source is comprised of multiple SMGs below our detection threshold. In this case, 2 or 3 SMGs marginally below the detection threshold at the edge of the FWHM primary beam ($S_{870} < 2$ mJy) would be sufficient to explain the missing flux in these maps, and we note that this would increase the fraction of multiples in our sample to about 70%.

While the presence of a ULIRG companion to the majority of the brightest SMGs is clearly significant, it is important to investigate the relative brightness of the secondary components, and the contribution they make to the flux density of the original SCUBA-2 detections. In Figure 5 we show the fraction of the integrated flux density in an ALMA map that is emitted by each SMG. We stress that the integrated flux density is the sum of the primary beam corrected flux densities of the SMGs in each ALMA map, and that this calculation does not take into account the effect of the SCUBA-2 beam. Where secondary components (i.e., fainter SMGs) are detected in an ALMA map, the ratio between brightest and secondary component is on average 25^{+1}_{-5}%, falling to 16% and 9% for the third and fourth components, respectively.

As shown in Figure 5 we do not see a significant trend in the fractional flux density of the secondary components with the single-dish flux density of the targeted submm sources. To quantify this statement split the sample into equal subsets at the median single-dish flux density of the sample ($S_{850} = 8.7$ mJy). The fainter subset of ALMA maps have on average 0.5 ± 0.2 secondary SMGs, compared to 1.2 ± 0.2 for the brighter subset (see Figure 5). Although the increased number of secondary SMGs in the ALMA maps of the brightest sub-mm sources tentatively suggests that brighter single-dish sources are comprised of a blend of a greater number of SMGs we caution against strong conclusions given the number of sub-mm sources considered in the analysis. As we note below this is broadly consistent with the theoretical results of Cowley et al. (2015) who predict that the brightest sub-mm sources are comprised of a marginally higher number of $S_{870} \gtrsim 1$ mJy SMGs.

Next, we investigate the ratio of the brightest component in each ALMA map to the original SCUBA-2 detection. We measure a median ratio of $S^{\rm ALMA}_{\rm Brightest}/S^{\rm SCUBA-2} = 0.80^{+0.06}_{-0.02}$, and do not find a significant trend in this ratio with single-dish flux (Figure 5). This result has important implications for studies that identify a single counterpart to the sub-mm emission from a single-dish source using emission at different wavelengths (e.g., 1.4 GHz); it suggests that even if the probabilistic identification is correct (see Hodge et al. 2013b) the true flux density of the SMG is on average 20% lower than the single-dish flux. Within the associated errors this is broadly consistent with the results of Cowley et al. (2015), who compared simulated single-dish and interferometric follow-up observations using the semi-analytic model GALFORM and predict that the brightest SMG comprises ~70% of the single-dish flux density.

We now compare our results to samples of interferometrically identified SMGs in the literature. Barger et al. (2012) present 860 μm SMA observations for a sample of 16 850 μm SCUBA-detected sources and find that 3 of the sources are comprised of multiple SMGs. As stated by those authors, the number of sources in the sample is small, and as the SMA maps reach a depth $\sigma_{860} \sim 0.7$–1 mJy, they are only sensitive to secondary SMGs brighter than 3–4 mJy (at the phase center). Similarly, Smolčić et al. (2012) found that 6 out of 28 LABOCA sources (870 μm selected) fragment into multiple components in 1.3 mm observations with the PdBI; in 9 of the PdBI maps no SMGs are detected. While this study again suggests that multiplicity is important, it is more challenging to interpret as the single-dish selection and interferometric follow-up observations were conducted at different wavelengths.

Recently, Hodge et al. (2013b) presented the results of an 870 μm ALMA survey of 122 single-dish sources detected in the 870 μm LABOCA survey of the Extended *Chandra* Deep Field South (LESS). The reader should note that the single-dish sub-mm sources studied by Hodge et al. (2013b) are on average 30% fainter than the sources presented here. From the 88 best quality ALESS maps (median $\sigma_{870} = 0.39$ mJy, with an interquartile range of 0.35–0.42 mJy), Hodge et al. (2013b) extract a sample of 117 SMGs. In 32 of the maps the single-dish detected sub-mm source fragments into multiple SMGs. While this indicates that the fraction of sub-mm sources that are blends of multiple SMGs is 35%, there are two caveats. First, 17 of the ALMA maps are blank, with the most likely reason being that the sub-mm source has fragmented into >2 SMGs below the detection threshold (Hodge et al. 2013b). Second, Hodge et al. (2013b) show that to recover the LABOCA flux density in the ALMA maps it is necessary to account for flux from sources below their detection threshold, indicating that a significant proportion of their ALMA maps contain faint 1–2 mJy SMGs, even though sources in this flux range should be rare in random patches of sky. Support for this conclusion comes from a stacking analysis of individually undetected IRAC galaxies in the ALMA maps, which shows that these galaxies are brighter in the sub-mm than expected for typical IRAC galaxies (Decarli et al. 2014).

To perform an accurate comparison between our sample and ALESS we remove the SMGs from our sample that lie below the ALESS detection threshold and repeat the multiplicity calculation. In total 13 SMGs are fainter than the ALESS threshold and are removed from our sample, resulting in an additional "blank" ALMA map (3/30). The fraction of "blank" maps in our sample is lower than that for the ALESS sample, which may simply reflect the significantly lower resolution of the beam-convolved LABOCA map (27.″2 FWHM) compared to SCUBA-2 (20.″5 FWHM). Of the 17 maps in our sample

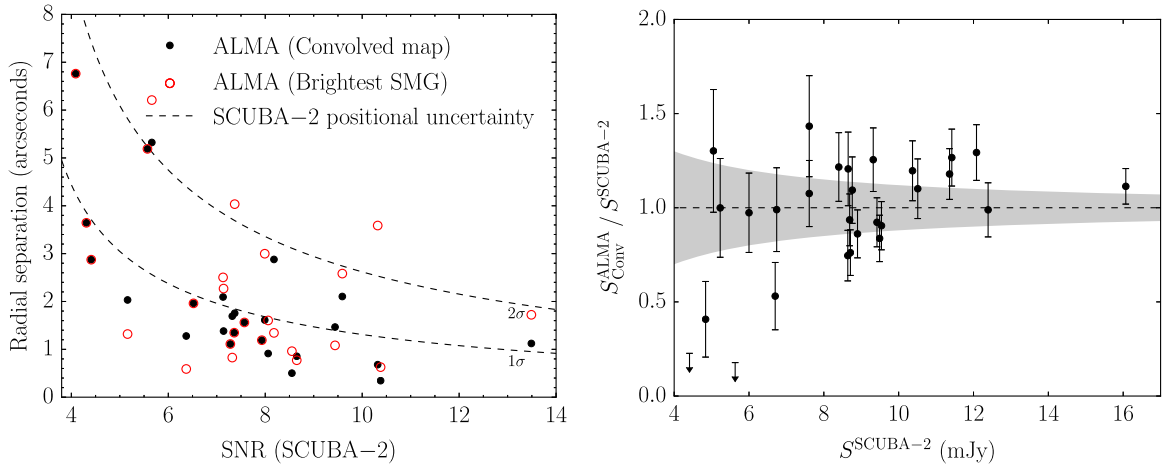

Figure 4. Left: we convolve the SMGs detected in each ALMA map with the SCUBA-2 beam and measure the positional offset between the flux centroid in the convolved map and the original single-dish-detected sub-millimeter source. The offset between the individual ALMA SMGs in each map and the single-dish source is also shown. The offsets between the ALMA convolved sources and the SCUBA-2 sources are consistent with the predicted uncertainty on the SCUBA-2 positions (see Ivison et al. 2007). Right: a comparison of the peak sub-mm emission from the SMGs detected in each ALMA map, convolved with the SCUBA-2 beam, and the SCUBA-2 flux density. The typical uncertainty on the SCUBA-2 flux densities is represented by the gray shaded region. We find good agreement between the SCUBA-2 and ALMA flux densities, with a median ratio of $S^{\rm ALMA}/S^{\rm SCUBA-2} = 0.99^{+0.10}_{-0.04}$. We do not detect any SMGs in two ALMA maps, but note that in both cases the SCUBA-2 single dish source is detected in *Herschel*/SPIRE imaging at 250, 350, and 500 μm indicating that these sources are real but potentially faint or multiple SMGs.

that contain multiple SMGs, 7 would have been classed as single identifications in the ALESS survey and 10 as multiples, yielding a multiplicity fraction of 37^{+15}_{-11}%. Hence, the fraction of single-dish sources classed as single identifications in our survey and ALESS are in close agreement.

To investigate any further differences between the samples we next compare the fraction of the single-dish flux density in the brightest component in each ALMA map. The median ratio of the observed flux densities in the ALESS sample is $S^{\rm ALMA}_{\rm Brightest}/S^{\rm LABOCA} = 0.64^{+0.06}_{-0.03}$, which is lower than our sample at a 2σ significance level ($S^{\rm ALMA}_{\rm Brightest}/S^{\rm SCUBA-2} = 0.80^{+0.06}_{-0.02}$). However, the larger beam size of LABOCA compared to SCUBA-2 means that secondary components contribute more to the single-dish detection. To test the effect of the beam size on the single-dish flux density we convolve a model of the SMGs in each ALMA map with the SCUBA-2 and LABOCA beams. We find that on average the LABOCA flux density is 2% higher than the SCUBA-2 detection, but stress that this is heavily weighted by the maps containing a single SMG (where the flux densities are identical) and that individual sources can be up to 13% brighter in the LABOCA observations. While this is clearly a small effect it does not include sources fainter than the ALMA detection threshold or outside the ALMA FWHM primary beam and should be considered a lower limit on the correction. Given all of the results above, we conclude that the sample presented here and by Hodge et al. (2013b) are broadly consistent.

4.2. Number Counts

The number counts of SMGs provide one of the most basic "observables," which galaxy formation models of the far-infrared universe must match. Recently, it has been suggested that the number of the brightest sub-mm sources ($S_{870} \gtrsim 9$ mJy) may have been over-estimated in single-dish studies (e.g., Karim et al. 2013) due to multiplicity. The single-dish sources in our sample are selected from the central 0.78 deg^2 of the S2CLS wide-field map of the UDS and have a median flux density of (8.7 ± 0.4) mJy. The sample is thus ideally suited to investigate the effects of multiplicity, and measure the intrinsic form of the bright-end of the number counts.

As discussed earlier our ALMA sample is increasingly incomplete for faint SCUBA-2 sources and so we choose to construct the number counts from our ALMA source catalog at $S_{870} > 7.5$ mJy.[18] To account for the incompleteness in our sample we first construct the counts from the ALMA observations assuming the selection is complete. For each ALMA-detected SMG we then correct the area surveyed based on the fraction of sources targeted in the flux bin of the parent single-dish sub-mm source.

In Figure 6 we show the differential and cumulative counts (Table 2) constructed from both our ALMA observations, and the parent SCUBA-2 sample (the uncertainty on the number counts are derived from Poisson statistics; see Gehrels 1986). As expected the ALMA number counts show a decrease relative to the single-dish counts; the intrinsic cumulative counts are 20% lower than the single-dish SCUBA-2 counts at $S_{870} > 7.5$ mJy, and 60% lower at $S_{870} > 12$ mJy.

Before discussing the shape and parameterization of the number counts, we first note that there is a difference between the bright-end of the number counts presented here, and the ALMA 870 μm counts derived from the ALESS survey (Karim et al. 2013). Our ALMA observations targeted 11 single-dish sources with flux densities >9 mJy and detect 7 SMGs above this threshold. In contrast, Karim et al. (2013) target 12 single-dish sources brighter than 9 mJy, but detect only 1 ALMA source above this threshold. The difference between these results may be due to multiplicity and the difference in the beam sizes of LABOCA and SCUBA-2 (see Section 4.1). However, it is important to note that the samples are small and are still dominated by small number statistics.

[18] The SMGs used to construct the number counts are detected at >15σ and all of the sources would have been detected in our maps, even at the edge of the primary beam.

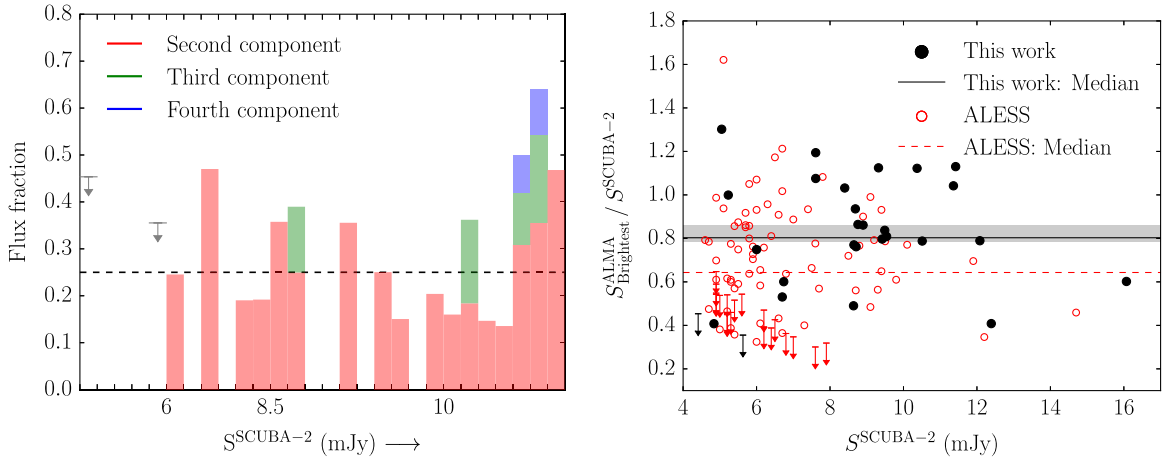

Figure 5. Left: in 61^{+19}_{-15}% of our ALMA maps the single-dish source targeted comprises of a blend of ⩾2 SMGs. Here we show the fraction of the total integrated flux in a map that is emitted by each individual SMG. Each interval on the abscissa represents an individual ALMA map, and the maps are ordered by increasing single dish flux density. Where an ALMA map contains >1 SMG the second component contributes on average 25^{+1}_{-5}% of the total flux (dashed line), with the third and fourth components contributing 16% and 9%, respectively. The two ALMA blank maps in our sample are represented by upper limits, placed at the maximum that a 4σ source at the edge of the ALMA primary beam could contribute to the SCUBA-2 flux density. Right: the fraction of the SCUBA-2 flux density emitted by the brightest SMG in each ALMA map, as a function of single-dish flux density. The median ratio for our sample is $S^{\rm ALMA}_{\rm Brightest}/S^{\rm SCUBA} = 0.80^{+0.06}_{-0.02}$ and we do not see a significant trend with single-dish flux density. Upper limits correspond to "blank" ALMA maps, and are the maximum contribution from a <4σ source located at the edge of the ALMA primary beam. For comparison we show the results from the ALESS survey (Hodge et al. 2013b), which found that 88 ALMA-identified LABOCA sub-mm sources have a median $S_{\rm Brightest}/S^{\rm LABOCA} = 0.64^{+0.06}_{-0.03}$. The lower fraction of flux density in the brightest component for the ALESS sample may be due to the combination of multiplicity and the larger beam size of LABOCA (27.″2), relative to SCUBA-2 (20.″5).

We now combine our sample with the ALESS survey (Karim et al. 2013), with the aim of providing a single parameterization of the intrinsic sub-mm number counts (Figure 6). To extend the range of the number counts to lower flux densities we also include two studies that have used serendipitous detections of sources in deep targeted ALMA observations to measure the number counts of faint SMGs at 1.2 and 1.3 mm from Ono et al. (2014) and Hatsukade et al. (2013), respectively. Although such studies are sensitive to clustering between the sources detected serendipitously and the original targets (which were not selected to be sub-mm sources), they do provide a crude estimate of the likely number counts of faint sources. We convert these counts to 870 μm using the composite SMG spectral energy distribution (SED) from the ALESS survey (see Swinbank et al. 2014), redshifted to $z = 2.5$ (flux conversion factors are 2.4× and 3.1 ×, at 1.2 mm and 1.3 mm, respectively). Although these converted faint number counts are sensitive to the shape of the adopted SED, they do appear to be in reasonable agreement with the cumulative counts from both this study, and ALESS (see Figure 6).

Since the number counts decline steeply at the bright-end we choose to model the counts with a double-power law of the form

$$N(>S) = \frac{N_0}{S_0}\left[\left(\frac{S}{S_0}\right)^{\alpha} + \left(\frac{S}{S_0}\right)^{\beta}\right]^{-1}, \quad (1)$$

where N_0 , S_0, α and β describe the normalization, break, and slope of the power laws, respectively. The best-fit parameters of the model are $N_0 = 390^{+110}_{-80}$ deg^{-2}, $S_0 = 8.4^{+0.6}_{-0.6}$ mJy, $\alpha = 1.9^{+0.2}_{-0.2}$, and $\beta = 10.5^{+3.0}_{-3.2}$, and as can be seen in Figure 6 the parameterization provides an adequate representation of the cumulative counts. However we caution that the number of sources at both the bright and faint end of the counts remains low (26 and 20 at $S_{870} < 2$ mJy and $S_{870} > 8$ mJy, respectively) and this is reflected in the uncertainties on the best-fit parameters.

When constructing the observed sub-mm number counts we have included three SMGs from our sample that we identify as potential gravitationally lensed sources (UDS 109.0, UDS 160.0, and UDS 269.0). All three of these SMGs appear to be close to, but spatially offset from, galaxies at $z \lesssim 1$ (see Simpson et al. 2015). Although there are no indications that these SMGs are strongly lensed (i.e., no multiple images), even a modest magnification of $\mu \geqslant 1.7$ is sufficient to push the intrinsic flux density of these sources below our threshold for constructing the number counts. If we remove these three SMGs then the cumulative number counts decrease by 18% at $S_{870} > 7.5$ mJy and the parameters of the best-fit double power law, for all of the ALMA samples, change by less than their associated 1-σ uncertainties.

It has been suggested that an absence of bright SMGs ($S_{870} \gtrsim 9$ mJy) may indicate a physical limit to the intense starbursts that are occurring in these sources (see Karim et al. 2013). We detect bright SMGs in our survey and do not find evidence for a sharp cut off in the counts. However, we do find that number counts decline strongly toward the bright-end with a distinct break at a flux density of $S_0 = 8.4^{+0.6}_{-0.6}$ mJy, which may suggest a typical threshold to the SFR. If we adopt the relationship between S_{870} and $L_{\rm FIR}$ for the ALESS SMGs (Swinbank et al. 2014), and the SMGs presented here (C.-J. Ma. et al. 2015, in preparation), then this break corresponds to a luminosity of $\sim 6 \times 10^{12}\, L_{\odot}$, or a SFR of $\sim 10^3$ $M_{\odot}$ yr^{-1} (for a Salpeter IMF). The SMGs in our sample are resolved in our ALMA imaging, and the brightest SMGs have a median half-light radius of 1.2 ± 0.1 kpc (Simpson et al. 2015). Given the sizes of the SMGs, the break in the number counts corresponds to a typical threshold to the SFR density in these starbursts of $\sim 100\, M_{\odot}$ yr^{-1} kpc^{-2}. The SFR

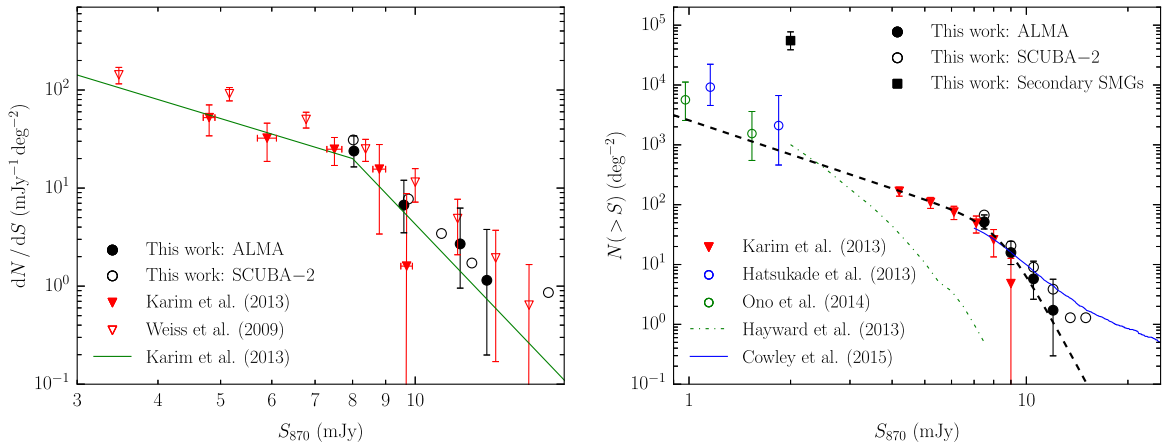

Figure 6. Left: the 870 μm differential counts constructed from our ALMA observations, compared to the parent single-dish SCUBA-2 sample. We also show the counts derived from the LABOCA, single-dish survey LESS (Weiß et al. 2009), and the counts from the follow-up ALMA survey ALESS (Karim et al. 2013). The counts derived from our survey are in agreement with the ALESS sample at $S_{870} \lesssim 9$ mJy and are well-described by a double-power law (see Section 4.2). We detect 7 SMGs with $S_{870} > 9$ mJy, compared to 1 SMG in ALESS, and do not see a sharp cut off in the counts, relative to the single-dish observations. Right: similar to the left panel, but instead showing the cumulative counts from the 870 μm surveys. The effect of multiplicity is more obvious in the cumulative counts and at $S_{870} > 7.5$ mJy the intrinsic counts from our ALMA survey are 20% lower than the counts from the parent single-dish sample, falling to 60% lower at $S_{870} > 12$ mJy. The cumulative counts from ALMA serendipitous detections at 1–1.3 mm, converted to 870 μm, are broadly in agreement with the sample presented here and from ALESS. We plot the best-fit double power-law function to all of the ALMA samples, which has a break at a characteristic flux density of $8.5^{+0.6}_{-0.6}$ mJy (dashed line). The theoretical predictions from Cowley et al. (2015) appear well-matched to the counts presented here. However, the counts presented by Hayward et al. (2013a) are least an order of magnitude lower than the observed counts at $S_{870} > 5$ mJy, which is attributed to the absence of "starbursts" in the model. The number density of secondary sources in ALMA maps with a primary SMG > 8 mJy (black square) is a factor of 80 ± 30 higher than the blank-field counts, which is inconsistent with these SMGs representing a line-of-sight population, and suggests that a significant fraction of these SMGs are physically associated.

density of a typical SMG at the break in the number counts is an order of magnitude lower than the expected Eddington limit for these sources (see Andrews & Thompson 2011; Simpson et al. 2015). However, we stress that the SFRs are integrated across the whole star-forming region. If the star formation in these SMGs is occurring in individual "clumps" (e.g., Danielson et al. 2011, 2013; Swinbank et al. 2011 then these individual regions may be Eddington limited, while the overall star-forming region appears sub-Eddington.

4.3. Comparison to Galaxy Formation Models

We now compare our results to recent theoretical predictions for sub-mm number counts, which attempt to simulate the effects of blending in single-dish surveys. Hayward et al. (2013a) construct single-dish and intrinsic sub-mm number counts, based on a hybrid numerical model. By construction the single-dish counts from the model are in broad agreement with single-dish observations at $S_{870} \sim 5$ mJy but, as shown in Figure 6, the intrinsic cumulative number counts under-predict the observed counts by over an order of magnitude at $S_{870} > 5$ mJy. As stated by Hayward et al. (2013a) the deficit is likely due to the absence of merger-driven "starbursts" in the model that act to elevate the star formation in these systems. We note that a previous model that includes "starbursts" is in closer agreement with the observed counts (see Hayward et al. 2013b). However, that model has a limited treatment of source blending and as shown in Hayward et al. (2013a) multiplicity has an order of magnitude effect on their predictions, which is not seen in our data.

In Figure 6 we also show the cumulative sub-mm counts from the semi-analytic model GALFORM (C.G. Lacey et al. 2015, in preparation) constructed using the simulations of single-dish and ALMA follow-up observations presented by Cowley et al. (2015). The current version of the model adopts an IMF in starbursts that is close to Salpeter, in contrast to previous versions that required a top-heavy IMF to describe SMGs (e.g., Baugh et al. 2005). In this new model the intense starbursts in SMGs are predominantly triggered by instabilities in gas-rich discs. To ensure a fair comparison to the counts presented here, we repeat the simulations presented in Cowley et al. (2015) but adopt the SCUBA-2 beam size and select sources with a flux density $\geqslant$7.5 mJy. As can be seen in Figure 6 the predicted follow-up counts from the model are in broad agreement with the counts presented here.

4.4. Origin of Multiplicity

A number of studies have investigated the environments of SMGs and concluded that the population are strongly clustered (Blain et al. 2004; Scott et al. 2006; Weiß et al. 2009; Hickox et al. 2012), although studies have questioned the robustness of these results (Adelberger 2005; Williams et al. 2011). Similarly, a small number of single-dish sources have been *resolved* into pairs of SMGs that have been spectroscopically confirmed to lie at the same redshift (e.g., Tacconi et al. 2006; Hodge et al. 2013a; Ivison et al. 2013). Such small scale over-densities of SMGs are unsurprising if these sources represent a population of massive galaxies, potentially undergoing merger induced star formation. Source multiplicity in SMGs thus offers one route to investigate the environments of these sources on scales up to 140 kpc (the FWHM primary beam of ALMA at $z \sim 2.5$).

The origin of multiplicity in SMGs can be conclusively tested through spectroscopic follow-up of the SMGs detected in each ALMA map. However, as we do not currently have spectroscopic redshifts for any of the SMGs in our sample we instead use the number density of sources fainter than the primary SMG in each ALMA map to assess their likely association. If these secondary SMGs are simply line-of-sight (LOS) projections, then, in the absence of any bias, the number density of sources should be equivalent to the background

counts. However, we must take into account the effect of blending on our initial sample selection, which will enhance the number of SMGs with companions in our target sample. Hence in the following analysis we *only* consider ALMA maps in our sample that contain an SMG brighter than 8 mJy. In doing so we ensure that we only consider the maps that would have been observed, regardless of whether blending with the detected companion boosts the flux density of the single-dish source into our sample.

There are 11 ALMA maps in our sample that contain an SMG brighter than 8 mJy, and we detect a total of 12 secondary SMGs in these maps. To derive the surface density of these SMGs we must adopt a flux limit for the sample. As the noise in the primary-beam corrected maps increases with distance from the phase center, and to ensure that we have uniform coverage, we first remove 1 secondary SMG with $S_{870} < 2$ mJy that would not have been detected at the edge of the ALMA primary beam. We calculate the area surveyed by the ALMA primary beam in these maps and measure that the cumulative number density of secondary SMGs brighter than 2 mJy is $(5.5^{+2.2}_{-1.6}) \times 10^4$ deg^{-2} and we show this point on Figure 6. In these 11 maps we expect to detect 0.14 SMGs at $S_{870} > 2$ mJy (adopting the blank field counts in Figure 6) but identify 11 SMGs. Therefore, the number density of the secondary sources in our maps is a factor of 80 ± 30 times higher than the blank field number counts, indicating that the brightest SMGs appear to reside in over-dense regions.

There is a small bias toward multiplicity in the selection of our single-dish sources that arises from observations of >8 mJy SMGs that, due to random noise fluctuations, scatter to lower values in the SCUBA-2 map. In such a scenario, an 8 mJy SMG is more likely to scatter back into our catalog if it has a companion SMG that boosts the single-dish flux density above our selection threshold. To determine the magnitude of this effect we use a simulation of single-dish observations of SMGs, presented by Cowley et al. (2015). To remove any intrinsic clustering in the simulation we randomize the positions of all of the input SMGs and then apply the sample selection described above. The resulting cumulative number density of secondary SMGs is a factor of 1.75 ± 0.75 times higher than the blank-field number counts. While this analysis confirms that our sample has a small bias due to noise, which increases the number of secondary SMGs, it is clearly insufficient to explain the magnitude of the observed offset.

Recently, theoretical predictions have been made for the origin of multiplicity of single-dish submm sources (see Hayward et al. 2013a; Cowley et al. 2015). In the simulations presented by Cowley et al. (2015), which are based on the semi-analytic model GALFORM, the majority of secondary SMGs are LOS projections, rather than physically associated sources. The apparent over-density of secondary SMGs in our maps may indicate that the brightest SMGs are more strongly clustered with fainter SMGs on ∼arcseconds scales than predicted by the model.

Clearly, to conclusively confirm these physical associations requires spectroscopic redshifts. We do not have spectroscopic redshifts for any of the SMGs in our sample, and as shown by Simpson et al. (2014) the photometric redshifts of SMGs have considerable uncertainties, ruling out the ability to perform this test with photometric redshifts alone. Moreover, only 35% of the secondary SMGs we have considered have a *K*-band counterpart (5σ detection limit 25.0 mag; see C.-J. Ma et al. 2015, in preparation). The only way to conclusively test if these sources are associated is through atomic or molecular emission spectroscopy (i.e., [C II], ^{12}CO) with sub-mm interferometry (see Weiß et al. 2013).

5. CONCLUSION

We have presented ALMA observations of 30 sub-mm bright single-dish sources in the UDS field. These sources were selected from 0.8 deg^2, 850 μm observations with SCUBA-2 at the JCMT as part of the S2CLS. The main conclusions from our study are as follows.

1. The 30 ALMA maps in our sample have a resolution of $0\farcs35 \times 0\farcs25$, and median noise of 0.21 mJy beam^{-1}. Using tapered versions of these maps (median resolution $0\farcs8 \times 0\farcs65$, $\sigma_{870} = 0.26$ mJy beam^{-1}) as detection images, we detect 52 SMGs at $>4\sigma$.
2. We find that 61^{+19}_{-15}% of the single-dish sub-mm sources in our sample are comprised of a blend of ⩾2 SMGs brighter than ≳1 mJy (i.e., multiple ULIRGs). On average the brightest SMG in each ALMA map comprises 80^{+6}_{-2}% of the single-dish flux density, and where a secondary SMG is detected it contributes 25^{+1}_{-5}% to the total integrated flux density in the ALMA map. In 2 of our maps we do not detect any SMGs, and in 10 maps we detect a single SMG. The remaining maps contain multiple SMGs, with 2, 3, or 4 SMGs detected in 14, 2 and 2 maps, respectively.
3. We compare our observations to the Cycle-0 ALMA survey of single-dish sources, ALESS. After accounting for the relative depths of both surveys we show that the fraction of sub-mm sources that are comprised of a blend of multiple individual SMGs is consistent, at ≳35%. However, in ALESS the brightest SMG in each ALMA map contains on average 65% of the single-dish flux density, compared to 80% for our sample. We show that this may be driven in part by the difference between the beam size of the initial single-dish selection for ALESS (LABOCA; beam-convolved FWHM = $27\farcs2$) and our survey (SCUBA-2; beam-convolved FWHM = $20\farcs5$).
4. We construct the differential and cumulative sub-mm counts of SMGs from our ALMA observations. The multiplicity bias in single-dish sources means that the intrinsic cumulative number counts are 20% lower at $S_{870} > 7.5$ mJy than the single-dish SCUBA-2 survey, and 60% lower at $S_{870} > 12$ mJy. We compare the counts derived from our survey to the theoretical models and demonstrate that the counts from the most recent GALFORM semi-analytic model (Cowley et al. 2015) are consistent with our results, at the flux density limit of our survey.
5. The number density of secondary SMGs ($S_{870} > 2$ mJy) around the brightest sources in our sample is 80 ± 30 times higher than expected from blank-field number counts. We caution that this result is still dominated by small number statistics, but we show that even after accounting for selection biases a significant fraction of these SMGs are likely to be physically associated. This suggests that the brightest SMGs reside in over-dense regions of SMGs

We thank Adam Avison and the Manchester ALMA ARC node for their assistance in verifying the calibration and

imaging of our ALMA data. J.M.S. acknowledges the support of STFC studentship (ST/J501013/1). A.M.S. acknowledges financial support from an STFC Advanced Fellowship (ST/H005234/1). I.R.S. acknowledges support from the ERC Advanced Investigator program DUSTYGAL 321334, an RS/Wolfson Merit Award and STFC (ST/I001573/1). J.E.G. acknowledges support from the Royal Society. R.J.I. acknowledges support from the European Research Council (ERC) in the form of Advanced Grant, COSMICISM 321302. E. Ibar acknowledges funding from CONICYT FONDECYT postdoctoral project No:3130504. K.K. acknowledges support from the Swedish Research Council. J.S.D. acknowledges the support of the European Research Council via the award of an Advanced Grant, and the contribution of the EC FP7 SPACE project ASTRODEEP (312725). I.A. acknowledges support from the grant CONACyT CB-2011-01-167291. This paper makes use of the following ALMA data: ADS/JAO. ALMA # 2012.1.00090.S. ALMA is a partnership of ESO (representing its member states), NSF (USA) and NINS (Japan), together with NRC (Canada) and NSC and ASIAA (Taiwan), in cooperation with the Republic of Chile. The Joint ALMA Observatory is operated by ESO, AUI/NRAO and NAOJ. This publication also makes use of data taken with the SCUBA-2 camera on the JCMT. The JCMT is operated by the Joint Astronomy Center on behalf of the Science and Technology Facilities Council of the United Kingdom, the National Research Council of Canada, and (until 31 March 2013) the Netherlands Organization for Scientific Research. Additional funds for the construction of SCUBA-2 were provided by the Canada Foundation for Innovation. All data used in this analysis can be obtained from the ALMA archive.

REFERENCES

Adelberger, K. L. 2005, ApJ, 621, 574
Alaghband-Zadeh, S., Chapman, S. C., Swinbank, A. M., et al. 2012, MNRAS, 424, 2232
Andrews, B. H., & Thompson, T. A. 2011, ApJ, 727, 97
Aravena, M., Younger, J. D., Fazio, G. G., et al. 2010, ApJL, 719, L15
Aretxaga, I., Wilson, G. W., Aguilar, E., et al. 2011, MNRAS, 415, 3831
Austermann, J. E., et al. 2010, MNRAS, 401, 160
Barger, A. J., Cowie, L. L., Sanders, D. B., et al. 1998, Natur, 394, 248
Barger, A. J., Wang, W.-H., Cowie, L. L., et al. 2012, ApJ, 761, 89
Baugh, C. M., Lacey, C. G., Frenk, C. S., et al. 2005, MNRAS, 356, 1191
Bertin, E., & Arnouts, S. 1996, A&AS, 117, 393
Bertoldi, F., Carilli, C., Aravena, M., et al. 2007, ApJS, 172, 132
Biggs, A. D., & Ivison, R. J. 2008, MNRAS, 385, 893
Biggs, A. D., Lvison, R. J., Ibar, E., et al. 2011, MNRAS, 413, 2314
Blain, A. W., Chapman, S. C., Smail, I., & Ivison, R. 2004, ApJ, 611, 725
Bothwell, M. S., Chapman, S. C., Tacconi, L., et al. 2010, MNRAS, 405, 219
Chapman, S. C., Blain, A. W., Smail, I., & Ivison, R. J. 2005, ApJ, 622, 772
Chapman, S. C., Smail, I., Windhorst, R., Muxlow, T., & Ivison, R. J. 2004, ApJ, 611, 732
Chen, C.-C., Cowie, L. L., Barger, A. J., et al. 2013, ApJ, 762, 81
Chen, C.-C., Cowie, L. L., Barger, A. J., et al. 2013, ApJ, 776, 131
Chen, C.-C., Smail, I., Swinbank, A. M., et al. 2015, ApJ, 799, 194
Coppin, K., Chapin, E. L., Mortier, A. M. J., et al. 2006, MNRAS, 372, 1621
Cowie, L. L., Barger, A. J., Wang, W.-H., & Williams, J. P. 2009, ApJL, 697, L122
Cowley, W. I., Lacey, C. G., Baugh, C. M., & Cole, S. 2015, MNRAS, 446, 1784
Danielson, A. L. R., Swinbank, A. M., Smail, I., et al. 2011, MNRAS, 410, 1687
Danielson, A. L. R., Swinbank, A. M., Smail, I., et al. 2013, MNRAS, 436, 2793
Dannerbauer, H., Walter, F., & Morrison, G. 2008, ApJL, 673, L127
Decarli, R., Smail, I., Walter, F., et al. 2014, ApJ, 780, 115
Dempsey, J. T., Friberg, P., Jenness, T., et al. 2013, MNRAS, 430, 2534
Eales, S., Lilly, S., Gear, W., et al. 1999, ApJ, 515, 518
Engel, H., Tacconi, L. J., Davies, R. I., et al. 2010, ApJ, 724, 233
Gear, W. K., Lilly, S. J., Stevens, J. A., et al. 2000, MNRAS, 316, L51
Gehrels, N. 1986, ApJ, 303, 336
Genzel, R., Baker, A. J., Tacconi, L. J., et al. 2003, ApJ, 584, 633
Greve, T. R., Ivison, R. J., Bertoldi, F., et al. 2004, MNRAS, 354, 779
Grev, T. R., Pope, A., Scott, D., et al. 2008, MNRAS, 389, 1489
Hainline, L. J., Blain, A. W., Smail, I., et al. 2011, ApJ, 740, 96
Hatsukade, B., Ohta, K., Seko, A., Yabe, K., & Akiyama, M. 2013, ApJL, 769, L27
Hayward, C. C., Behroozi, P. S., Somerville, R. S., et al. 2013, MNRAS, 434, 2572
Hayward, C. C., Narayanan, D., Kereš, D., et al. 2013, MNRAS, 428, 2529
Hickox, R. C., Wardlow, J. L., Smail, I., et al. 2012, MNRAS, 421, 284
Hodge, J. A., Carilli, C. L., Walter, F., Daddi, E., & Riechers, D. 2013, ApJ, 776, 22
Hodge, J. A., Karim, A., Smail, I., et al. 2013, ApJ, 768, 91
Hogg, D. W., & Turner, E. L. 1998, PASP, 110, 727
Hughes, D. H., Serjeant, S., Dunlop, J., et al. 1998, Natur, 394, 241
Ikarashi, S., Kohno, K., Aguirre, J. E., et al. 2011, MNRAS, 415, 3081
Iono, D., Peck, A. B., Pope, A., et al. 2006, ApJL, 640, L1
Ivison, R. J., Greve, T. R., Dunlop, J. S., et al. 2007, MNRAS, 380, 199
Ivison, R. J., Greve, T. R., Serjeant, S., et al. 2004, ApJS, 154, 124
Ivison, R. J., Greve, T. R., Smail, I., et al. 2002, MNRAS, 337, 1
Ivison, R. J., Smail, I., Le Borgne, J.-F., et al. 1998, MNRAS, 298, 583
Ivison, R. J., Swinbank, A. M., Smail, I., et al. 2013, ApJ, 772, 137
Karim, A., Swinbank, A. M., Hodge, J. A., et al. 2013, MNRAS, 432, 2
Laurent, G. T., Aguirre, J. E., Glenn, J., et al. 2005, ApJ, 623, 742
Lawrence, A., Warren, S. J., Almaini, O., et al. 2007, MNRAS, 379, 1599
Lilly, S. J., Eales, S. A., Gear, W. K. P., et al. 1999, ApJ, 518, 641
Lindner, R. R., Baker, A. J., Omont, A., et al. 2011, ApJ, 737, 83
Magnelli, B., Lutz, D., Santini, P., et al. 2012, A&A, 539, A155
Menéndez-Delmestre, K., Blain, A. W., Swinbank, M., et al. 2013, ApJ, 767, 151
Ono, Y., Ouchi, M., Kurono, Y., & Momose, R. 2014, ApJ, 795, 5
Pope, A., Borys, C., Scott, D., et al. 2005, MNRAS, 358, 149
Scott, S. E., Dunlop, J. S., & Serjeant, S. 2006, MNRAS, 370, 1057
Scott, S. E., Fox, M. J., Dunlop, J. S., et al. 2002, MNRAS, 331, 817
Simpson, J. M., Smail, I., Swinbank, A. M., et al. 2014, ApJ, 788, 125
Simpson, J. M., Smail, I., Swinbank, A. M., et al. 2015, ApJ, 799, 81
Smail, I., Ivison, R. J., & Blain, A. W. 1997, ApJL, 490, L5
Smail, I., Ivison, R. J., Owen, F. N., Blain, A. W., & Kneib, J.-P. 2000, ApJ, 528, 612
Smolčić, V., Aravena, M., Navarrete, F., et al. 2012, A&A, 548, A4
Swinbank, A. M., Chapman, S. C., Smail, I., et al. 2006, MNRAS, 371, 465
Swinbank, A. M., Papadopoulos, P. P., Cox, P., et al. 2011, ApJ, 742, 11
Swinbank, A. M., Simpson, J. M., Smail, I., et al. 2014, MNRAS, 438, 1267
Swinbank, A. M., Smail, I., Chapman, S. C., et al. 2010, MNRAS, 405, 234
Tacconi, L. J., Genzel, R., Smail, I., et al. 2008, ApJ, 680, 246
Tacconi, L. J., Neri, R., Chapman, S. C., et al. 2006, ApJ, 640, 228
Toft, S., Smolčić, V., Magnelli, B., et al. 2014, ApJ, 782, 68
Wang, W.-H., Cowie, L. L., Barger, A. J., & Williams, J. P. 2011, ApJL, 726, L18
Wang, W.-H., Cowie, L. L., van Saders, J., Barger, A. J., & Williams, J. P. 2007, ApJL, 670, L89
Weiß, A., De Breuck, C., Marrone, D. P., et al. 2013, ApJ, 767, 88
Weiß, A., Kovács, A., Coppin, K., et al. 2009, ApJ, 707, 1201
Williams, C. C., Giavalisco, M., Porciani, C., et al. 2011, ApJ, 733, 92
Younger, J. D., Fazio, G. G., Ashby, M. L., et al. 2010, MNRAS, 407, 1268
Younger, J. D., Fazio, G. G., Huang, J.-S., et al. 2007, ApJ, 671, 1531
Younger, J. D., Fazio, G. G., Huang, J.-S., et al. 2009, ApJ, 704, 803